Quantum walk of light in frequency space and its controlled dephasing

Deepak Pandey, Nandan Satapathy, M. S. Meena, and Hema Ramachandran*
Raman Research Institute, Sadashivanagar, Bangalore 560080, India
(Received 11 May 2011; published 11 October 2011)

We implement, using a coherent source, a coined quantum walk of light in frequency space in a tabletop experiment utilizing a series of modified Michelson interferometers that incorporate polarization optics and acousto-optic modulators. Manipulating the phase of the radio frequency that governs the acousto-optic interaction, we achieve symmetric or asymmetric quantum walks. Introducing rapid random phase shifts electronically, while regulating the amplitude, we cause controlled dephasing and thus simulate a gradual transition from the quantum walk to the classical random walk.

DOI: 10.1103/PhysRevA.84.042322 PACS number(s): 42.50.Ex, 42.25.Hz, 05.40.Fb, 78.20.H−

I. INTRODUCTION

A discrete quantum walk is an analog of a classical random walk where the quantum nature of both the coin and the walker is manifest and the classical probabilities are replaced by probability amplitudes. In other words, the coin and the walker can each be in a superposition state of its corresponding basis vectors, and the probability amplitudes of various possible paths of the walker interfere. This results in the probability distributions of the quantum walker being quite distinct from that of a classical random walker. Ever since their introduction [1–3] there has been immense interest in quantum walks [4,5], motivated by the promise of faster execution of a variety of computational tasks [6–9]. It has now been shown that any quantum circuit can be effectively simulated by continuous [10] or discrete quantum walks [11], making them universal computational primitives. Quantum walks have also been invoked to explain the efficiency of photosynthesis [12]. A related area of current interest, both from the theoretical point of view and from the practical implementation angle, is the transition from the quantum walk to the classical random walk, brought about by decoherence [13–22].

Quantum walks have been experimentally demonstrated in a variety of systems: ions [23,24], single atoms [25], spin systems [26,27], and light [28–33]. Of these, light and photons are of particular interest, as they are relatively easy to produce, control, and measure. There are numerous ways of manipulating light. Do *et al*. [31] used an array of beam splitters, and Perets *et al*. [32] an array of waveguides, to demonstrate the quantum walk of light in real space. Using holographic phase plates, Zhang and coworkers [33] showed the quantum walk of light in orbital angular momentum space. Recent studies by Schreiber *et al*. [28] examined the quantum walk of photons in time. The optical Galton board experiment by Bouwmeester [34], done in a different context, has been subsequently interpreted as a quantum walk of light in frequency space [35]. Interest in the quantum walk of light is rapidly increasing. Recent experiments have investigated the quantum walk of correlated photons [30] and the transition from the quantum to the classical [29,36].

In this paper we implement up to four steps of a quantum walk of light in discrete frequency space using a cascade of modified Michelson interferometers (MMIs) that incorporate polarization optics and acousto-optic modulators (AOMs). Exercising a fine control over the phase of the light, we go from an asymmetric to a symmetric quantum walk. More importantly, by introducing rapid random phase shifts, dephasing of the walk to various extents is achieved, leading to a gradual transition to the classical random walk behavior. Finally, a multipass scheme is discussed that simplifies the experimental arrangement for single photons for a larger number of steps of the walk.

II. DISCRETE QUANTUM WALKS

Typically, the Hilbert space for the one-dimensional quantum walk is defined by a two-state coin basis and a one-dimensional discrete position space. The state of the walker is given by

$$\Psi = \frac{\sum_{n=-\infty}^{+\infty} (a_n|n \otimes X\rangle + b_n|n \otimes Y\rangle)}{\sqrt{\sum_{n=-\infty}^{+\infty} (a_n^2 + b_n^2)}}, \quad (1)$$

where $|X\rangle$ and $|Y\rangle$ represent the two basis states of the coin and n denotes the position in space. A single step of the quantum walk is defined by the sequential operation of C, the Hadamard coin operator, which is given by

$$C = \sum_{n=-\infty}^{+\infty} |n\rangle\langle n| \otimes (|X+Y\rangle\langle X| + |X-Y\rangle\langle Y|)/\sqrt{2}, \quad (2)$$

and D, the conditional displacement, which is given by

$$D = \sum_{n=-\infty}^{+\infty} |n+1\rangle\langle n| \otimes |X\rangle\langle X| + |n-1\rangle\langle n| \otimes |Y\rangle\langle Y|. \quad (3)$$

The N-step unbiased Hadamard walk is given by $(DC)^N$. By suitably altering C and D while maintaining unitarity, quantum walks of different kinds may be realized.

The outcome of a quantum walk is quite different from that of a classical random walk in several respects. For example, for an N-step classical random walk, the positional probability distribution of the walker is maximum at the origin, and the standard deviation goes as $\sqrt{N}$. In contrast, the probability

*hema@rri.res.in

distribution is suppressed at the origin (due to interference) in the quantum walk and is peaked at the edges, with a standard deviation varying linearly with N. The walker thus spreads more rapidly; hence the importance of the quantum walk for search algorithms. The outcome of a classical random walk, because of the stochastic nature, is independent of the initial state of the walker. The outcome of a quantum walk, on the other hand, is governed by the initial state; for example, symmetric or asymmetric walks result depending on whether the initial state was $(|0 \otimes X\rangle + |0 \otimes Y\rangle)/\sqrt{2}$ or $(|0 \otimes X\rangle + i|0 \otimes Y\rangle)/\sqrt{2}$. Further, being a unitary evolution, the quantum walk is reversible, while the classical random walk is not.

III. QUANTUM WALK OF LIGHT

A. Scheme for the quantum walk of a photon

Figure 1 depicts an MMI, which is the basic building block of our quantum walk setup. Here the symmetric beam splitter of a conventional Michelson interferometer is replaced by a polarizing beam splitter (PBS) and each arm of the interferometer has an AOM. The AOM $A+$, in one arm, up-shifts the frequency of the photon, and $A-$, in the other, down-shifts the frequency by the same amount. Thus the combination of the PBS and the AOMs enables state-dependent displacement

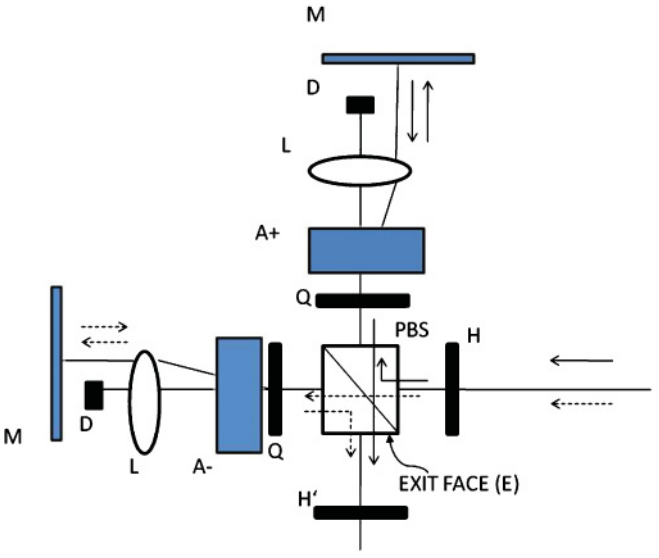

FIG. 1. (Color online) Schematic of a modified Michelson interferometer (MMI): solid and dashed arrows depict the path of two orthogonal polarization components, X and Y. Light is shown entering the MMI from the right. H is a half-wave plate, with its fast axis at 22.5° to the $|X\rangle$ polarization, used to achieve a Hadamard operation; PBS is a polarizing beam splitter; and Q's are quarter-wave plates that have their fast axes at 45° to the $|X\rangle$ polarization. A+ and A− are frequency up-shifting and frequency down-shifting acousto-optic modulators, D's are beam dumps used to stop the undiffracted light, L's are lenses placed such that the acousto-optic modulators are at their focus, and M's are mirrors that are normal to the optical axis and are placed at a focal distance behind the lens. H′ is a half-wave plate at 45° to $|X\rangle$, used to flip the polarization of the light emerging from face E. This compensates for the flip in polarization that light suffers on the double transit through quarter-wave plates Q.

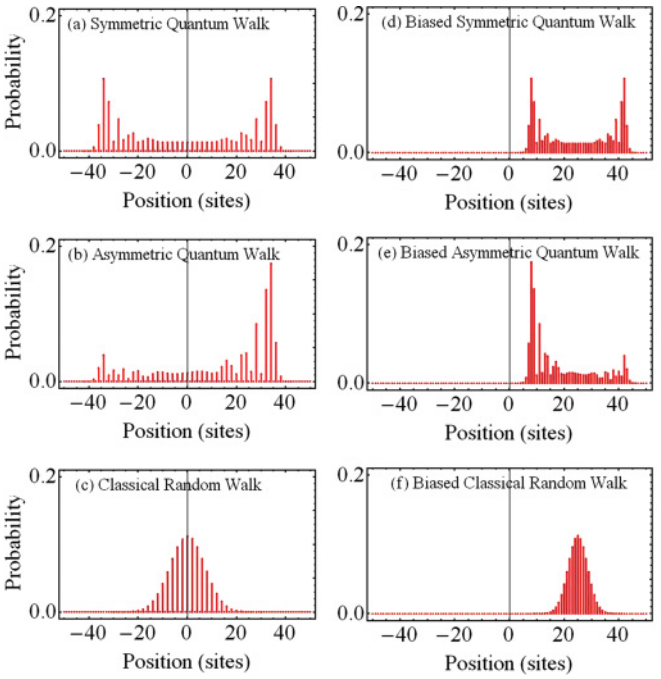

FIG. 2. (Color online) Probability distribution of a walker after 50 steps of different walks: (a) quantum walk with initial state $(|0 \otimes X\rangle + i|0 \otimes Y\rangle)/\sqrt{2}$; (b) quantum walk with initial state $|0 \otimes X\rangle$; (c) classical random walk; (d) biased quantum walk with initial state $(|0 \otimes X\rangle + i|0 \otimes Y\rangle)/\sqrt{2}$; (e) biased quantum walk with initial state $|0 \otimes X\rangle$; (f) biased classical random walk. For the D operation in (a) and (b), Eq. (3) is used, while in (d) and (e) Eq. (6) is used.

in frequency space. A half-wave plate, with the fast axis at an angle of 22.5° to the vertical, is inserted before the PBS, so as to obtain a Hadamard coin. By rotating the half-wave plate, the bias of the coin may be altered. Quarter-wave plates Q in the two arms of the MMI serve to bring the polarization of the photon in each arm at exit to a state orthogonal to that at entry into the arm. This ensures that the photons, after executing a step in frequency space, exit through face E of the PBS. The AOMs are in a standard "double-pass" configuration. With $(|0 \otimes X\rangle$ as input, the output after H' will be $(|1 \otimes X\rangle + |-1 \otimes Y\rangle)/\sqrt{2}$. Thus traversal of an MMI by a photon constitutes a single step of the quantum walk. A multistep quantum walk can be executed in a cascade of such MMIs.

In order to reduce the number of optical components in our implementation we have removed the AOM from one of the arms of each MMI and the HWP at the exit face; i.e., A− and H′ in Fig. 1 were removed, while A+ and H were retained. This in no way alters the underlying nature of the walk, though some changes do occur. As only one polarization component executes a displacement in frequency space, the walk is biased to one side; this is equivalent to a shift of the origin with each step. The number of occupied sites remains the same but there is a reduction in the frequency spread by a factor of 2. This biased displacement operator is given by

$$B = \sum_{n=-\infty}^{+\infty} |n+1\rangle\langle n| \otimes |X\rangle\langle X| + |n\rangle\langle n| \otimes |Y\rangle\langle Y|. \quad (4)$$

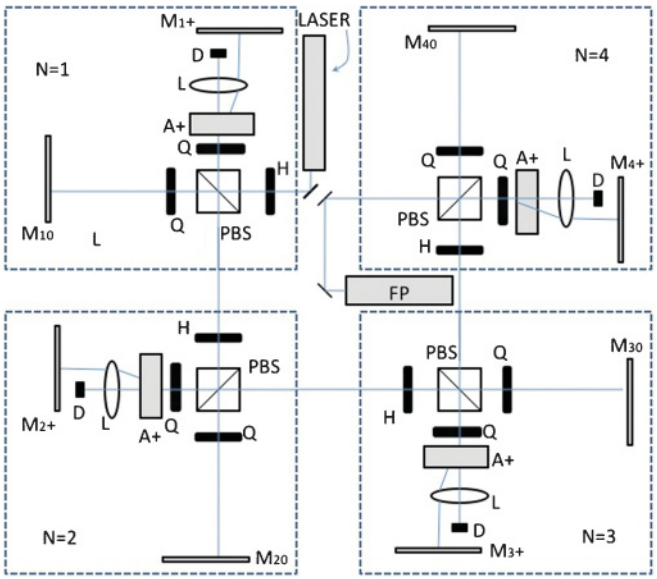

FIG. 3. (Color online) Experimental setup for a four-step quantum walk. Each dashed box constitutes a step of the walk. Note that only one arm of each MMI has an AOM and that H′ of the MMI (Fig. 1) has been removed; this reduces the requirement on the optics.

The removal of the half-wave plate H′ at the exit face is equivalent to the introduction of a flip operator defined by

$$F = \sum_{n=-\infty}^{+\infty} |n\rangle\langle n| \otimes (|Y\rangle\langle X| + |X\rangle\langle Y|). \tag{5}$$

Hence for our implementation we have $D = FB$, given by

$$D = \sum_{n=-\infty}^{+\infty} |n\rangle\langle n| \otimes |X\rangle\langle Y| + |n+1\rangle\langle n| \otimes |Y\rangle\langle X|. \tag{6}$$

The expected outcomes of the standard Hadamard quantum walk [Eqs. (2) and (3)] and our implementation [Eqs. (2) and (6)] are shown in Fig. 2, for 50 steps of the walk. Also given are the outcomes for classical random walks, with and without a bias for displacement.

We have implemented a four-step quantum walk [$(DC)^4$, with D as in Eq. (6) and C as in Eq. (2)] using a cascade of four MMIs as shown in Fig. 3. We performed the experiment using coherent light, as both coherent light and single photons are expected to yield the same results in a quantum walk [37,38].

B. Experimental details

Our experiment employed a single-mode, narrow-linewidth laser light at 767 nm (Toptica DLX) and AOMs (Isomet), driven by a radio-frequency (rf) signal from a versatile frequency generator (VFG 150). The spectrum was analyzed using a scanning Fabry-Perot interferometer (FPI). The output light from the FPI was collected on a photodetector, suitably amplified, and displayed on a fast digital storage oscilloscope. About 30 mW of laser light was input to the MMI cascade. The AOMs were operated at 80 MHz; in double-pass geometry, the frequency of light is shifted by 160 MHz, which we denote as one step in frequency space. The experiment was controlled by LabVIEW. We use a coherent source of light, although the scheme is suited for a single-photon implementation as well. We note here that both coherent light and single photons are expected to yield the same results in a quantum walk [37,38].

The cascade of interferometers, being mechanically very sensitive, had to be shielded from air drafts and vibrations. For alignment of the various components we found the following steps to be crucial. First, the two paths within each stage were matched by viewing the interference pattern at the exit of a stage. For this the AOM was switched off (to avoid frequency mismatch), the beam dump was removed (to allow the undiffracted light to pass), and a glass plate was introduced at the exit to reflect off a small part of the light to a screen. A polarizer (at 45° to the vertical) kept in front of the screen permits interference between light from the the two arms. Mirror M2 was adjusted to obtain a single bright fringe on the screen. (A bright fringe corresponds to light beams from both arms exiting the stage in phase, and a dark fringe corresponds to the two beams being exactly out of phase. Permitting both bright and dark fringes on to a detector for measurement would then wash out the interference effect, as, in that case, an average intensity distribution would be obtained.)

The AOM was then switched on, and the spectrum of the light from a single stage was viewed using the FPI. As the AOMs operate typically at 80%; efficiency (which, on double pass, reduces to about 60%;), the beams in the two arms suffer unequal loss, as only one of them passes through an AOM. To compensate for this and other losses (e.g., arising due to imperfect polarization optics), filters were appropriately introduced, to ensure that the two peaks, as seen using the FPI, were of equal heights. The paths were then matched across stages, with the AOMs switched on. These being in double-pass configuration, the exit path of light is not altered whether or not the AOM is switched on. For example, to match paths across MMI-1 and MMI-2, we examined the light exiting the second stage using the FPI, initially with mirror M_{1+} and mirror M_{20} blocked, then with these unblocked and M_{10} and mirror M_{2+} blocked instead. The alignment was adjusted till the spectra in both cases were identical. In a similar fashion, paths across all pairs of MMIs were aligned.

It is imperative that all rf signals be synchronized to a common clock to ensure frequency and phase matching. A slight mismatch in frequencies of two of the AOMs gives rise to beats in the interference of light beams emerging from these AOMs. During alignment, the frequencies were intentionally mismatched, and the alignment optimized for the largest beat signal. Once aligned, the frequencies were set exactly equal.

C. Results of an *N*-step quantum walk

The results of our experiment are shown in Fig. 4, as an array of frames. In each frame, given as a bar graph, is the expected intensity distribution at different frequencies, as calculated using Eqs. (2) and (6). Superimposed on these, in the form of line plots, are the normalized intensities as measured using the scanning FPI. The first column shows the outcome of an N-step quantum walk, the second column gives the contribution from the $|X\rangle$-polarized component, and the third column that of the $|Y\rangle$-polarized component. N increases as we go down a column. As noted earlier, a single step of the quantum walk is the sequential operation of C and D. At the right, next

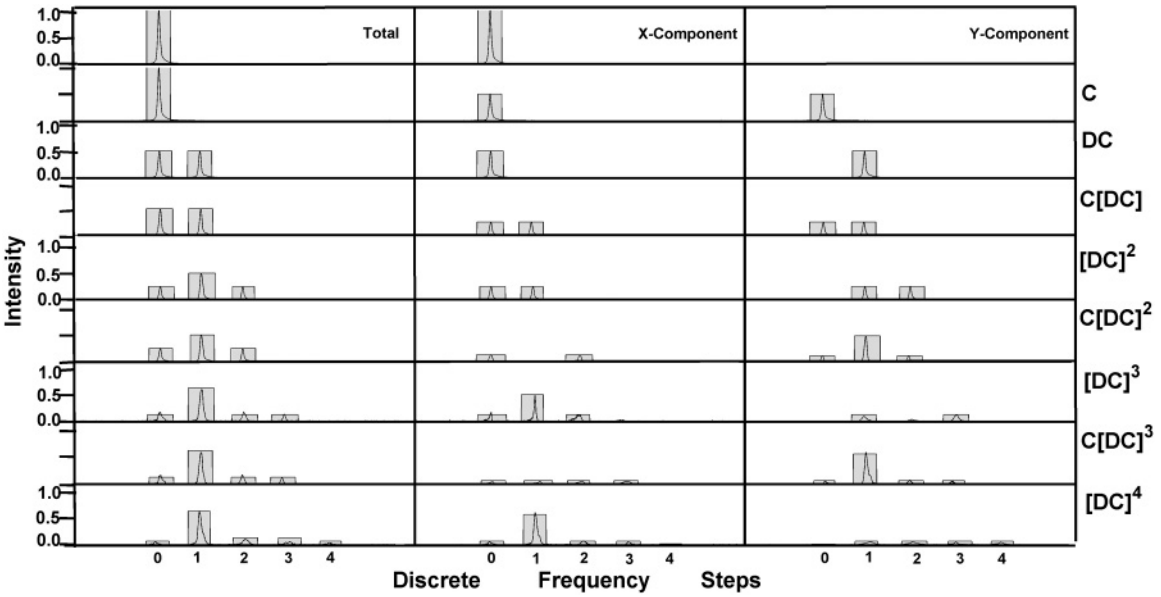

FIG. 4. Theoretically expected (gray bar) and experimentally obtained (bold curve) outcomes for various steps of the quantum walk in Fig. 3, with initial state $|X\rangle$. The nine rows represent different stages of the walk, as indicated at the right. The total intensity and those of the X-polarized and Y-polarized components are given in the different columns. The experimentally obtained curves are the normalized Fabry-Perot measurement of a single scan.

to each row, is given the sequence of operations that were performed to obtain the intensities given in that row. The match between theory and experiment is good; the deviations from the expected values arise mainly from the imperfect polarization optics.

The input state of light in this experiment was $|X\rangle$. The operator C serves to redistribute the total intensity into the two components $|X\rangle$ and $|Y\rangle$, while the D serves to shift it in frequency space (see, e.g., the second and third rows in Fig. 4). The interference therefore occurs at the C operation. This is clearly illustrated in Fig. 4. As shown, the first indication of interference occurs at $C(DC)^2$. Comparing the frames in the rows $(DC)^2$ and $C(DC)^2$, we see that the distribution of the total intensity is peaked at frequency 1 and looks like that of a classical random walk. However, the intensity of the $|X\rangle$ component in $C(DC)^2$ shows a suppression at frequency 1 and that for the $|Y\rangle$ component shows an enhancement at the same frequency over the values in the previous row. This may be understood as follows: on the completion of steps $(DC)^2$, the $|X\rangle$ component has equal probability at frequencies 0 and 1, and the $|Y\rangle$ at frequencies 1 and 2. Though both the $|X\rangle$ and the $|Y\rangle$ components have nonzero amplitude at frequency 1, no interference takes place, as they are mutually orthogonal. In a subsequent operation of C, both $|X\rangle$ and $|Y\rangle$ go into superposition states, permitting interference. Thus, the resulting probability amplitude [after $C(DC)^2$] has a cancellation in the $|X\rangle$ polarization and a reinforcement in the $|Y\rangle$ polarization. By the next step $(DC)^3$, the asymmetric nature of the walk is evident in the total intensity.

IV. PHASE MANIPULATION

A phase shift may be imparted to light in an interferometer by altering the path length, e.g., by moving the end mirror or introducing a phase retarder. To avoid mechanical operations, and to enable rapid phase shifts, we make use of the acousto-optic interaction, where the introduction of a phase shift of θ to the rf being fed to the AOM will cause the phase of the nth-order diffracted light to shift by $n\theta$. Light traversing the AOM arms of our MMIs suffer a first-order diffraction twice, and thus we can impart a 2θ phase shift by applying a θ phase shift to the rf. Exploiting this transfer of phase from the rf to light, we have made a transition from a symmetric to an asymmetric walk and have also introduced controllable dephasing, as discussed below. In fact, this method permits the introduction of identical or nonidentical phase shift to any select number of AOMs in the setup.

A. Transition from a symmetric to an asymmetric quantum walk

Linearly polarized light gives rise to an asymmetric walk, with the displacement being peaked at the high-frequency or the low-frequency side, depending on whether the input was polarized along the $|X\rangle$ or the $|Y\rangle$. On the other hand, with circularly polarized light as the input, a symmetric walk is expected. Usually, the change in linear polarization is achieved by use of a half-wave plate, while the introduction of helicity is achieved by use of a quarter-wave plate. These retard one component with respect to the other. In our experiment, the outcomes after the first step (DC) for the various input states are

$$DC|0 \otimes X\rangle = \frac{1}{\sqrt{2}}|0 \otimes X\rangle + \frac{1}{\sqrt{2}}|1 \otimes Y\rangle, \tag{7}$$

$$DC|0 \otimes Y\rangle = -\frac{1}{\sqrt{2}}|0 \otimes X\rangle + \frac{1}{\sqrt{2}}|1 \otimes Y\rangle, \tag{8}$$

$$DC\left|0 \otimes \frac{X + iY}{\sqrt{2}}\right\rangle = \frac{1-i}{2}|0 \otimes X\rangle + \frac{1+i}{2}|1 \otimes Y\rangle. \tag{9}$$

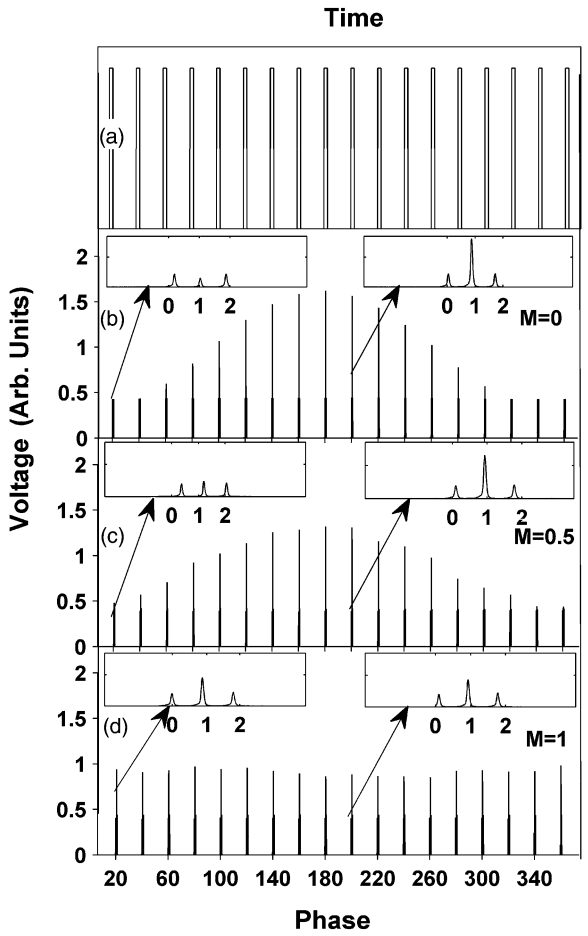

FIG. 5. Oscilloscope traces, as a function of time, to show the effect of the phase noise. (a) Voltage vs time of the trigger pulses. The trigger pulse increments the phase difference between the AOMs in MMI-1 and MMI-2 by $10^\circ + M\delta\phi(t)$, where M lies between 0 and 1 and $\delta\phi(t)$ is a string of random values between -90° and 90°. The corresponding phase shift suffered by light passing through the AOM is twice as much due to the double-pass. The numbers at the bottom indicate the phase shift of light with $M = 0$. (Only the upward ramp is shown.) The output of the Fabry-Perot is given as function of time for the cases (b) $M = 0$, (c) $M = 0.5$, and (d) $M = 1$. Insets: The expanded waveform of a single scan of the Fabry-Perot showing peaks at three distinct frequencies. Both from the envelope of (b), (c), and (d) and from the insets, the transition from the quantum (b) to the classical (d) is evident with increased dephasing.

We note that in all the cases, the $|X\rangle$ component is at frequency 0, while the $|Y\rangle$ component is at frequency 1 after the first step. The difference in the outcomes for the various input polarizations is only the relative phase between the $|X\rangle$ and the $|Y\rangle$ components. In our implementation, the same phase retardation or phase advance may be obtained electronically by introducing a phase shift in the rf to the AOM in the first MMI. Thus a transition from the left asymmetric walk, to the symmetric walk, to the right asymmetric walk can be achieved electronically. This effect has been illustrated in Fig. 5, which is explained in detail in the following section.

B. Controlled dephasing

In a similar fashion, dephasing of the walk may be effected by introducing arbitrary independent phase shifts to the rf inputs to the various AOMs. As the first signature of the quantum walk appears after operation $C(DC)^2$, in the form of a suppression of the central peak in the $|X\rangle$ component and a corresponding enhancement in the $|Y\rangle$ component, we illustrate the transition from the quantum to the classical behavior at this stage. White noise of the desired amplitude is sampled (at short intervals, $t = 500$ ns) and added to the phase of the rf input of one of the two AOMs, leading to relative dephasing of the light components passing through them. By controlling the amplitude of the white noise, dephasing of the quantum walk to different extents is achieved and a gradual transition from the quantum walk behavior to that for a classical random walk is demonstrated. The results are shown in Fig. 5, which includes four oscilloscope traces. The topmost trace [Fig. 5(a)] is the trigger pulse, which occurs at regular intervals, $T = 2$ ms. This causes two things to happen.

(1) A shift in phase, by an amount $10^\circ + M\delta\phi(t)$, is introduced to the rf in one of the AOMs. Here M, the amplitude of the phase noise, lies between 0 and 1; $\delta\phi(t)$, the phase deviation, is a string of random values between -90° and 90° and changes very rapidly, i.e., $t \ll T$.

(2) A single scan of the FPI is initiated, of duration T. The frequency range of the scan is much larger than the frequency spread of the walker. As $T \gg t$ (i.e., the period of the scan is much larger than the time scale of the random phase jumps), the scan is essentially a time-averaged recording.

Figures 5(b)–5(d) are the signals recorded for different values of M when the light, after the operation $C(DC)^2$, is directed through an $|X\rangle$ polarizer onto the scanning FPI. Figure 5(b) gives the result for the case $M = 0$, that is, when there is no relative noise between the two MMIs. Each trigger pulse increments the phase of the rf to one AOM by 10°. We recall here that the phase shift suffered by light is twice that applied to the rf. The oscilloscope trace shows a number of spikes. Each spike actually consists of the three peaks recorded during a single scan of the FPI; the insets give the expanded trace. Initially, the central peak is suppressed, as is expected in the quantum walk for the $|X\rangle$ component after the operation $C(DC)^2$. If we advance the phase of the AOM in the first MMI by $\pi/2$ (phase of light by π), the outcome should be what would have been obtained had the input been $|Y\rangle$. This is exactly what we obtain when a 180° phase shift has been applied to the light. An additional phase shift of 180° to the light once again gives the outcome expected for the $|X\rangle$ component. When a 90° phase shift has been applied to light in one of the MMIs, the output obtained corresponds to the quantum walk of circularly polarized light. In this case (i.e., $C(DC)^2$), both the $|X\rangle$ and the $|Y\rangle$ polarized components have the same resultant intensities. For a larger number of steps, the distribution of intensity over frequency for the $|X\rangle$ component is the mirror image of that for the $|Y\rangle$ component.

Figure 5(c) gives the output of the FPI for $M = 0.5$. The contrast in the fringes (relative peak heights, i.e., interference in frequency space) has decreased. In Fig. 5(d), the phase noise has increased in amplitude to $M = 1$, and the walk is now classical: no interference takes place. The output is independent of the relative phase shifts.

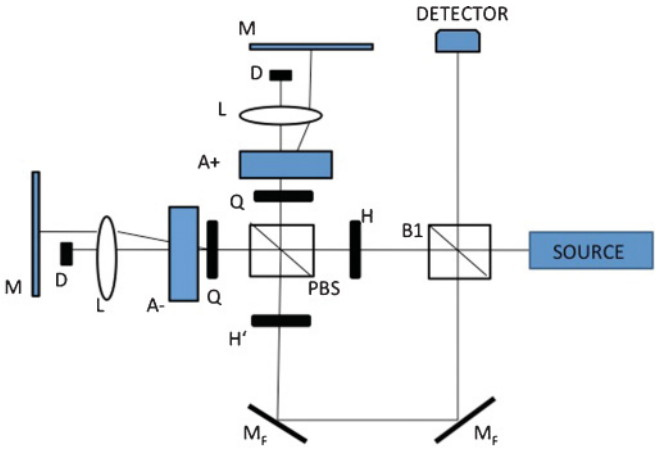

FIG. 6. (Color online) Multipass modified Michelson interferometer scheme for a compact implementation of the quantum walk of light in frequency space. B1 is a nonpolarizing beam splitter with a high reflectivity; H is a half-wave plate, with its fast axis at 22.5° to the $|X\rangle$ polarization, used to achieve a Hadamard operation; PBS is a polarizing beam splitter; and Q's are quarter-wave plates that have their fast axes at 45° to the $|X\rangle$ polarization. A+ and A− are frequency up-shifting and frequency down-shifting acousto-optic modulators, D's are beam dumps used to stop the undiffracted light, L's are lenses placed such that the acousto-optic modulators are at their focus, M's are mirrors that are normal to the optical axis, and M_F's are mirrors used to fold the path of light and effect the multipass.

V. DISCUSSION

Our implementation of the quantum walk utilizes a coherent source. The use of a single-photon source would make our realization a truly quantum walk. The easiest method to do this would be to use a highly attenuated light source and postselect events that satisfy the existence of a single photon in the setup.

In the present experimental setup, the number of optical components increases linearly as N, the number of steps in the walk. Further, to achieve a quantum-to-classical transition for an N-step quantum walk, all interfering paths have to be decohered, requiring independent phase control of ∼N AOMs. Both of these disadvantages can be eliminated by the implementation of a folded geometry as shown in Fig. 6. This has a single MMI with two additional mirrors and a nonpolarizing beam splitter with a high reflectivity. Photons may reach the detector after $0,1,2,\ldots,N$ steps. The time taken for a photon to complete an N-step walk is $\tau = N\tau_I + \tau_S + \tau_D$, where τ_I is the time taken for a photon starting from the beam splitter B_1 to return to the same point, having made a single transit of the MMI, τ_S is the time of travel from the source to B_1, and τ_D from B_1 to the detector. Photons may be injected at a rate less than $1/\tau$ and the random phase-shifts timed to within $1/\tau_I$ intervals to target individual steps. By careful path matching of path lengths and beam alignment, one may ensure a cavity implementation leading to higher probabilities for walks with a large number of steps. The limited efficiency of AOMs (∼60%; in the double-pass configuration) would be the main source of loss in MMI-based schemes.

After N steps, a classical walk has a probability distribution peaked at the center, while a quantum walker has it peaked at the end(s). A more uniform spread of the quantum walker is obtained when a small amount of decoherence is introduced [14]. This uniform spread is of importance in search-based algorithms. Our experiment provides a way of introducing decoherence via dephasing in a controlled manner, and is both rapid and amenable to electronic control. With the ability to give different phase shifts to the two basis states, one can easily create time-dependent coins and time-dependent walk steps and anisotropic walks.

The quantum walk of a photon in frequency space is an ideal way of creating a photon in a superposition of frequency states. Interaction of such a photon with a multilevel atom would give rise to many interesting variants of superposition and entanglement, of possible utility in practical applications like quantum logic gates. For such atom-light entanglement, a few steps of a quantum walk, as in our experiment, would suffice, as selection rules for dipole transitions restrict the number of allowed transitions.

ACKNOWLEDGMENTS

We wish to acknowledge the help of Mr. Somasekhar in the initial stages of the work on introduction of rf phase shifts and the help of Mr. Sourish Banerjee with some of the LabVIEW programming. We also thank Andal Narayanan for stimulating discussions.

[1] S. Godoy and S. Fujita, J. Chem. Phys. **97**, 5148 (1992).
[2] Y. Aharonov, L. Davidovich, and N. Zagury, Phys. Rev. A **48**, 1687 (1993).
[3] E. Farhi and S. Gutmann, Phys. Rev. A **58**, 915 (1998).
[4] J. Kempe, Contemp. Phys. **44**, 307 (2003).
[5] V. Kendon, Philos. Trans. R. Soc. A **364**, 3407 (2006).
[6] A. M. Childs, R. Cleve, E. Deotto, E. Farhi, S. Gutmann, and D. A. Spielman, *Proceedings, 35th ACM Symposium on Theory of Computing* (2003), p. 5968, e-print arXiv:quant-ph/0209131; A. M. Childs, L. J. Schulman, and U. V. Vazirani, in *Proceedings, 48th IEEE Symposium on Foundations of Computer Science* (2007), p. 395–404, e-print arXiv:0705.2784.
[7] A. Ambainis, SIAM J. Comput. **37**(1), 210 (2007).
[8] F. Magniez, M. Santha, and M. Szegedy, in *Proceedings, 16th ACM-SIAM Symposium on Discrete Algorithms* (2005), p. 1109–1117, e-print arXiv:quant-ph/0310134.
[9] E. Farhi, J. Goldstone, and S. Gutmann, Theory Comput. **4**(1), 169 (2008).
[10] A. M. Childs, Phys. Rev. Lett. **102**, 180501 (2009).
[11] N. B. Lovett, S. Cooper, M. Everitt, M. Trevers, and V. Kendon, Phys. Rev. A **81**, 042330 (2010).
[12] M. Mohseni, P. Rebentrost, S. Lloyd, and A. Aspuru-Guzik, J. Chem. Phys. **129**, 174106 (2008).
[13] T. A. Brun, H. A. Carteret, and A. Ambainis, Phys. Rev. Lett. **91**, 130602 (2003).
[14] V. Kendon and B. Tregenna, Phys. Rev. A **67**, 042315 (2003).

[15] A. Romanelli, R. Siri, G. Abal, A. Auyuanet, and R. Donangelo, Physica A **347**, 137 (2004).
[16] J. Kosik, V. Buzek, and M. Hillery, Phys. Rev. A **74**, 022310 (2006).
[17] N. V. Prokofev and P. C. E. Stamp, Phys. Rev. A **74**, 020102(R) (2006).
[18] A. C. Oliveira, R. Portugal, and R. Donangelo, Phys. Rev. A **74**, 012312 (2006).
[19] V. Kendon, Math. Struct. Comput. Sci. **17**, 1169 (2007).
[20] Y. Yin, D. E. Katsanos, and S. N. Evangelou, Phys. Rev. A **77**, 022302 (2008).
[21] J. D. Whitfield, C. A. Rodriguez-Rosario, and A. Aspuru-Guzik, Phys. Rev. A **81**, 022323 (2010).
[22] R. Srikanth, S. Banerjee, and C. M. Chandrashekar, Phys. Rev. A **81**, 062123 (2010).
[23] F. Zahringer, G. Kirchmair, R. Gerritsma, E. Solano, R. Blatt, and C. F. Roos, Phys. Rev. Lett. **104**, 100503 (2010).
[24] H. Schmitz, R. Matjeschk, Ch. Schneider, J. Glueckert, M. Enderlein, T. Huber, and T. Schaetz, Phys. Rev. Lett. **103**, 090504 (2009).
[25] M. Karski, L. Forster, J.-M. Choi, A. Steffen, W. Alt, D. Meschede, and A. Widera, Science **325**, 174 (2009).
[26] J. Du, H. Li, X. Xu, M. Shi, J. Wu, X. Zhou, and R. Han, Phys. Rev. A **67**, 042316 (2003).
[27] C. A. Ryan, M. Laforest, J. C. Boileau, and R. Laflamme, Phys. Rev. A **72**, 062317 (2005).
[28] A. Schreiber, K. N. Cassemiro, V. Potocek, A. Gabris, P. J. Mosley, E. Andersson, I. Jex, and Ch. Silberhorn, Phys. Rev. Lett. **104**, 050502 (2010).
[29] M. A. Broome, A. Fedrizzi, B. P. Lanyon, I. Kassal, A. Aspuru-Guzik, and A. G. White, Phys. Rev. Lett. **104**, 153602 (2010).
[30] A. Peruzzo *et al*., Science **329**, 1500 (2010).
[31] B. Do, M. L. Stohler, S. Balasubramanian, D. S. Elliot, C. Eash, E. Fischbach, M. A. Fischbach, A. Mills, and B. Zwickl, J. Opt. Soc. Am. B **22**, 499 (2005).
[32] H. B. Perets, Y. Lahini, F. Pozzi, M. Sorel, R. Morandotti, and Y. Silberberg, Phys. Rev. Lett. **100**, 170506 (2008).
[33] P. Zhang, X.-F. Ren, X.-B. Zou, B.-H. Liu, Y.-F. Huang, and G.-C. Guo, Phys. Rev. A **75**, 052310 (2007).
[34] D. Bouwmeester, I. Marzoli, G. P. Karman, W. Schleich, and J. P. Woerdman, Phys. Rev. A **61**, 013410 (1999).
[35] P. L. Knight, E. Roldan, and J. E. Sipe, Phys. Rev. A **68**, 020301(R) (2003).
[36] A. Schreiber, K. N. Cassemiro, V. Potocek, A. Gabris, I. Jex and Ch. Silberhorn, Phys. Rev. Lett. **106**, 180403 (2011).
[37] V. Kendon and B. C. Sanders, Phys. Rev. A **71**, 022307 (2005).
[38] P. P. Rohde, A. Schreiber, M. Stefanak, I. Jex, and C. Silberhorn, New J. Phys. **13**, 013001 (2011).